Italian Journal of Engineering Geology and Environment
www.ijege.uniroma1.it

ASSESSMENT OF SLOPE PROCESSES IN A DEEP-SEATED ROCKSLIDE-EARTHSLIDE BY INTEGRATED INVESTIGATION AND MONITORING: BRUGNETO CASE STUDY (NORTHERN APENNINES, ITALY)

Cecilia FABBIANI(*), Marco MULAS(*), Benedikt BAYER(**), Vincenzo CRITELLI(***), Silvia FRANCESCHINI(**), Irene GHISELLI(****), Francesco LELLI(*), Melissa TONDO(*), Giovanni TRUFFELLI(****) & Alessandro CORSINI(*)

(*)*Università Degli Studi di Modena e Reggio Emilia - Dipartimento di Scienze Chimiche e Geologiche - Modena (Italy)*
(**)*Fragile Srl - Bologna (Italy)*
(***)*Autorià di Bacino Distrettuale del Fiume Po - Parma (Italy)*
(****)*Agenzia per la sicurezza territoriale e la protezione civile - Piacenza (Italy)*
Corresponding author: cecilia.fabbiani@unimore.it

EXTENDED ABSTRACT

Lo studio presenta un'analisi integrata dei processi di versante che interessano la frana profonda di Brugneto, localizzata nell'Appennino Settentrionale (bacino del Trebbia, provincia di Piacenza, Emilia-Romagna), con l'obiettivo di ricostruirne la struttura interna, la cinematica e i fattori di controllo, a supporto della valutazione della pericolosità. Le frane profonde a cinematica lenta rappresentano uno dei principali agenti geomorfologici responsabili dell'evoluzione del paesaggio appenninico e costituiscono un elemento critico per la gestione del rischio, soprattutto in contesti caratterizzati da elevata complessità geologica e strutturale. La frana di Brugneto, estesa su circa 1,18 km² con un dislivello di circa 500 m, è classificata nel Piano di Assetto Idrogeologico del Fiume Po come area a pericolosità molto elevata (R3–R4) e interessa direttamente nuclei abitati. Il corpo di frana si sviluppa prevalentemente all'interno del Flysch di Monte Caio, in un contesto strutturale a assetto variabile, che risulta localmente a franapoggio nel settore di distacco, favorevole all'innesco del movimento. L'approccio metodologico si basa sull'integrazione di dati preesistenti e nuovamente acquisiti mediante diverse tecniche di monitoraggio, sia a terra che da remoto.

In particolare, sono stati utilizzati: (*i*) un DTM ad alta risoluzione derivato da rilievo UAV-LiDAR per l'analisi morfologica e la mappatura geomorfologica; (*ii*) una tomografia elettrica di resistività (ERT) longitudinale alla direzione di movimento del corpo di frana per la caratterizzazione della sua struttura interna; (*iii*) sondaggi profondi attrezzati ad inclinometri per l'identificazione delle superfici di scivolamento multiple; (*iv*) un sistema di monitoraggio GNSS continuo (2023-oggi) per la misura degli spostamenti superficiali; (*v*) analisi InSAR multi-temporali (RAINS e MT-SBAS) basate su immagini satellitari Sentinel-1 per la ricostruzione dell'evoluzione deformativa di lungo periodo (2014-2024).

L'integrazione dei dataset ha consentito di suddividere il corpo di frana in tre principali sub-unità, caratterizzate da differenti meccanismi di movimento, materiali e tassi di spostamento. La frana mostra una transizione cinematica da scivolamenti rotazionali in roccia nel settore superiore ad uno scivolamento traslativo in terra nel piede di frana, dove si registrano le velocità più elevate.

Le superfici di scivolamento principali rilevate raggiungono profondità fino a 70 m, come evidenziato dall'integrazione dei dati inclinometrici e geofisici. Il monitoraggio GNSS evidenzia un incremento progressivo delle velocità di spostamento dal coronamento verso il piede della frana, con valori massimi nella sub-unità inferiore. Inoltre, in questo settore è evidente dall'analisi combinata tra spostamento superficiale e dati pluviometrici una chiara correlazione tra fasi di accelerazione e periodi di precipitazioni cumulative prolungate. I risultati InSAR risultano coerenti dal punto di vista qualitativo con i dati GNSS, pur mostrando una sottostima delle velocità nelle aree a maggiore deformazione, confermando la necessità di un approccio integrato tra tecniche satellitari e misure a terra. La carta geomorfologica e la sezione geologica prodotte costituiscono un modello interpretativo robusto della frana di Brugneto, evidenziando come l'architettura interna e le relazioni tra le sub-unità controllino la variabilità spaziale della cinematica. Lo studio dimostra l'efficacia dell'integrazione di più sistemi di monitoraggio per la comprensione delle frane profonde e complesse, fornendo un valido riferimento per la valutazione della pericolosità e la pianificazione di strutture di mitigazione in contesti geologici analoghi dell'Appennino Settentrionale o simili altrove.

IJEGE, Special Issue 1, (2026): 83-95, DOI: 10.4408/IJEGE.2026-01.S-08
E-ISSN 2035-5688 | ISSN 1825-6635 / ©Author(s)

ABSTRACT

This study defines the reference geological model of the Brugneto deep-seated landslide (Northern Apennines, Piacenza province, Italy). An integrated mapping and monitoring approach reconstructs its internal structure and kinematics and defines its controlling factors for hazard assessment purposes. The landslide affects an area of approximately 1.18 km² and develops mainly within the Monte Caio Flysch, in a structurally complex dip-slope setting. Specifically, the study integrates UAV-LiDAR derived DTM analysis, electrical resistivity tomography, boreholes logging, inclinometers, continuous GNSS monitoring, and multi-temporal InSAR analyses (RAINS and MT-SBAS) based on Sentinel-1 data. This multi-source approach allowed the identification of three main landslide sub-units, characterized by different materials, movement mechanisms, and displacement rates. Results show a kinematic transition from rotational rock sliding in the upper sector to translational earth sliding in the lower sector. Sliding surfaces reach depths of 70 m. GNSS data reveal increasing displacement rates toward the lower landslide sector and a clear relationship between acceleration phases and prolonged rainfall periods. InSAR data are consistent with ground-based measurements but tend to underestimate velocities in the most active areas. The resulting landslide map and cross sections represent the reference geological model for this complex landslide while the adopted study approach can be replicated in similar geological settings.

Keywords: *deep-seated landslide, Northern Apennines, integrated monitoring, landslide mapping, geological model.*

INTRODUCTION

Deep-seated landslides are among one of the primary geomorphic agents responsible for landscape evolution in the northern Apennines of Italy (Corsini *et alii*, 2005; Borgatti et al., 2006; Crosta *et alii*, 2013; Bertolini *et alii*, 2017). Specifically, in the Piacenza province (Emilia-Romagna Region), the landslide spatial frequency ratio is 28.4%, and some municipalities can reach up to 50% or more. Most of the landslides are Very Slow (≤1.6 m/yr) to Extremely Slow (≤16 mm/yr) (Cruden & Varnes, 1996).

In general, analysing long-term deformation processes in large, complex, deep-seated landslides is essential for reliable hazard and risk assessment, as well as for identifying effective mitigation measures (Guzzetti *et alii*, 1999; Carrara *et alii*, 2003; Van Westen *et alii*, 2003; Corominas *et alii*, 2014; Roccati *et alii*, 2021). Also, to achieve a comprehensive understanding of internal structure and active kinematics a multi-source data integration approach is generally adopted (Agliardi et al., 2001; Van Westen & Lulie Getahun, 2003; Bonzanigo *et alii*, 2007; Corsini *et alii*, 2015; Del Soldato *et alii*, 2018; Pastor *et alii*, 2019; Simeoni *et alii*, 2020). This is because of the intrinsic complexity of large deep-seated landslides, which arises from their size, volume, and spatially heterogeneous movement mechanisms (Petley & Allison, 1997; Zangerl *et alii*, 2010), as well as from the interaction of geological, hydrological, and morphological factors controlling their temporal behaviour (Pánek & Klimeš, 2016; Wieczorek G.F., 2016; Lacroix *et alii*, 2020).

Furthermore, integrating multiple datasets also allows a detailed understanding and accurate mapping of landslide processes, which are essential for reconstructing their spatio-temporal evolution and for supporting hazard assessment within the landslide body, particularly in relation to its internal zonation (Pasuto & Soldati, 1999; Lee, 2001; Parry, 2011; Guzzetti *et alii*, 2012; Tofani *et alii*, 2014; Sacchini *et alii*, 2016; Mulas *et alii*, 2018; Chelli *et alii*, 2021; Donnini *et alii*, 2025). In this context, high-resolution topographic data derived from LiDAR and DTM analyses have proven to be particularly effective for detecting geomorphological features, delineating landslide boundaries and internal sub-units, and supporting the reconstruction of slope deformation processes (Dewitte & Demoulin, 2005; Sterzai *et alii*, 2010; Jaboyedoff *et alii*, 2012; Johnson *et alii*, 2023; Ciccarese *et alii*, 2024; Lelli *et alii*, 2025).

This study deals with the application of a multi-source data integration approach for the definition of the reference geological model of the Brugneto landslide (Northern Apennines, municipality of Ferriere, Province of Piacenza, Italy) (Fig. 1). The study evidences how geological features influence the characteristics of slope instability processes that, in turn, are reflected on differentiated displacement rates along the slope. The findings also offer a reference operational framework for similar slope deformation processes in the Northern Apennines or comparable geological settings elsewhere, for hazard assessment and the design of targeted mitigation strategies.

MATERIALS AND METHODS

Study area

The Brugneto landslide, in the Trebbia river-basin, covers an area of 1.18 km² and extends from 1077 m a.s.l. to 575 m a.s.l., with a total relief of about 500 m. It is a site classified at very high hydrogeological risk (R3 and R4) by the Po-river Basin Hydrogeological Asset Plan (PAI-Po, PS267), since the landslide affects the settlements of: Brugneto (at 900 m a.s.l.), and Casale Brugneto (at 720 m a.s.l.). The area is included in Sheet 197 "Bobbio" of the 1:50,000 Geological Map of Italy (Elter *et alii*, 1997). The area lies within the so-called "Bobbio Window," a tectonically and stratigraphically significant structural domain in the Northern Apennines. The outcropping formations belong to the Ligurian Units and the subordinate Sub-Ligurian Units (Fig. 1). Specifically, the landslide develops almost entirely within the Monte Caio Flysch, a turbidite made of alternating limestones, marls and pelites.

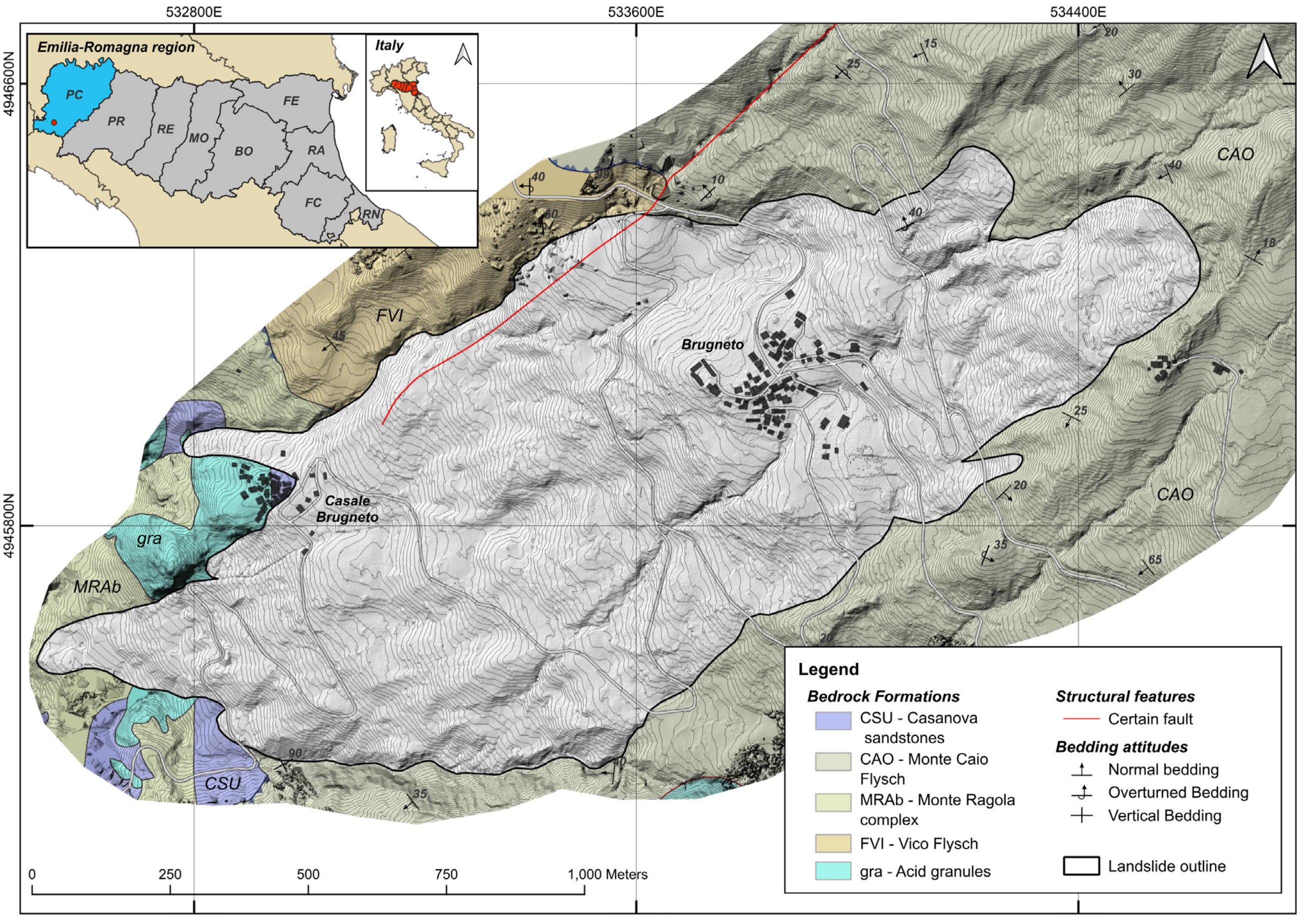

Fig. 1 - Geographic location of the Brugneto landslide and general geological setting of the slope (Geological Map of the Emilia-Romagna Region, 1:10,000 scale)

At the landslide toe, the Casanova Sandstones crop out, consisting of arenaceous-pelitic turbidites containing ophiolitic clasts. Both units are part of the Caio-Ottone Tectonic Succession. To achieve a detailed geological characterization of the Brugneto landslide, available datasets were integrated with new data acquired through different monitoring systems.

Terrain dataset

A Digital Terrain Model (DTM) with a spatial resolution of 1 m was used in this study. The DTM was derived from a drone-based LiDAR survey carried out in 2022 and served as the primary topographic dataset for the analysis. It was used to generate hillshade maps supporting the identification and mapping of landslide sub-units, as well as to extract elevation profiles employed in the construction of the reference geological cross-sections.

Underground dataset

A 1435 m long longitudinal electrical resistivity tomography (ERT1) profile was acquired in December 2022 across the landslide, crossing the Brugneto hamlet (Fig. 2). The survey employed 288 electrodes with 5 m spacing and a Wenner-Schlumberger array, a configuration widely adopted in landslide investigations (Jongmans & Garambois, 2007; Arosio *et alii*, 2011; Luhn *et alii*, 2023). This dataset was fundamental for reconstructing the internal structure of the landslide body.

Two additional ERT profiles (ERT2-3) were later collected in the Casale Brugneto area to refine the local subsurface characterization (Fig 2). Oriented transverse to the landslide body, they are less representative than the longitudinal profile but still provide useful complementary information. The ERT2, acquired with 96 electrodes spaced at 2.0 m, reached an investigation depth of 30 m, whereas the shorter ERT3, with 48 electrodes at the same spacing, investigated depths of about 15 m. Both surveys adopted Wenner-type quadripole configurations.

Subsurface information was further constrained by borehole data collected between December 2023 and January 2024. Borehole 5P was drilled with continuous coring to a depth of 21.0 m, whereas boreholes 4I (60.0 m) and 6I (71.5 m) were executed

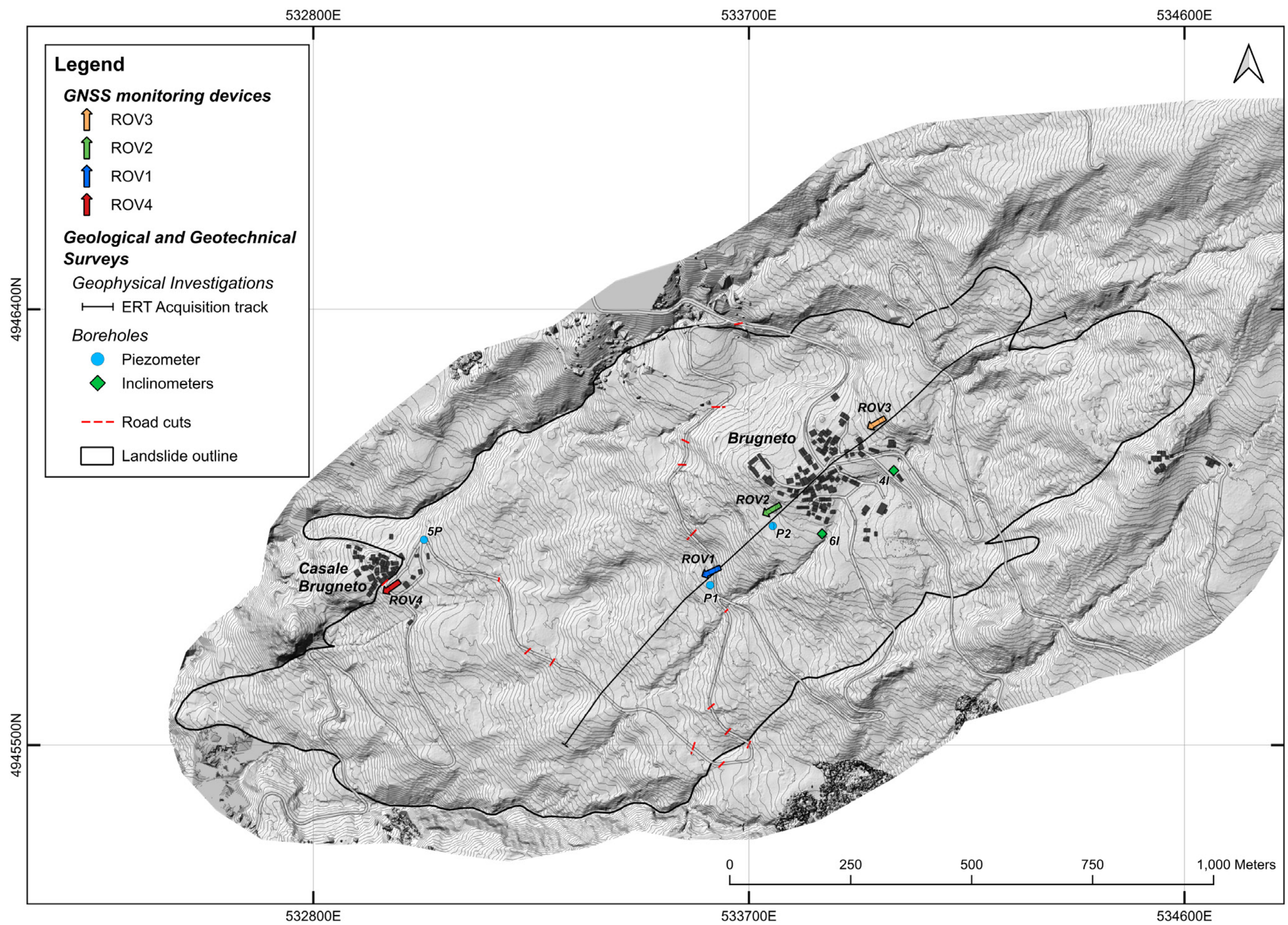

Fig. 2 - Map with location of underground investigation and monitoring locations

using a mixed technique, combining destructive drilling in the upper sections with continuous coring at depth (30-60 m for 4I; 60-71.5 m for 6I). A 150 cm long, 101 mm diameter single core barrel was used throughout, and all drillings were performed with a MASSENZA rotary rig (model MI 9 R).

Two additional continuously cored boreholes (P1 and P2) were also considered. Although details on drilling procedures are not available, their stratigraphic logs contributed to the reconstruction of subsurface conditions within the landslide area.

For kinematic monitoring, boreholes 4I and 6I were equipped with inclinometers, supporting the identification of active shear surfaces at depth. Measurements started in April 2024 and were repeated in May 2025, July 2025, and January 2026. Groundwater conditions were monitored through three piezometers. P1 (20 m deep) and P2 (40 m deep), installed in November 2022, were screened at 14-20 m and 34-40 m depth, respectively, in downslope and upslope positions relative to the Brugneto hamlet.

Borehole 5P was subsequently completed as a piezometer (installed in January 2024), screened between 15 and 21 m, with a cement-sealed blind casing up to ground level. All piezometers were equipped with piezoresistive pressure transducers recording groundwater level and temperature at 12-hour intervals.

Overall, the integrated geophysical, stratigraphic, and monitoring dataset provides a consistent framework for defining the lithological setting, the geometry of the main and secondary shear surfaces, and the spatial and kinematic relationships between landslide sub-units and the underlying bedrock.

Continuous GNSS monitoring

A continuous Global Navigation Satellite System (C-GNSS) monitoring system is operated in Brugneto since November 2023. It is based on Emlid Reach+ receivers and RTK correction approach (Mulas *et alii*, 2020b). The system consists of four rover stations installed along the landslide (from top to bottom: ROV3, ROV2, ROV1, and ROV4) and a master station in a stable position south of the landslide. The C-GNSS datasets provide continuous data on slope movements, thus supporting the interpretation of its deformation behaviour

(Glabsch *et alii*, 2009; Corsini *et alii*, 2015; Mulas *et alii*, 2020a; Mantovani *et alii*, 2022).

InSAR analysis

An Interferometric Synthetic Aperture Radar (InSAR) analysis was carried out for the time-period October 2014 to March 2024. The analysis is based on Sentinel-1 data (Massonnet & Feigl, 1998; Bürgmann *et alii*, 2000; Rosen *et alii*, 2000) and two different processing approaches:

- Interferogram Stacking (*i.e.* Rapid Areal InSAR Survey RAINS), suitable for detecting displacement rates ranging from 30 to 500 mm/yr along the Line of Sight (LOS) (Roering *et alii*, 2009; Squarzoni *et alii*, 2020; Ciuffi *et alii*, 2023), with a quasi-continuous spatial coverage of deformation patterns.
- Multi-Temporal In-SAR (*i.e.* Multi-Temporal Small Baseline Subset, MT-SBAS), suitable for detecting displacement rates ranging from 5 to 100 mm/yr (Berardino *et alii*, 2002; Schmidt & Bürgmann, 2003; Lanari *et alii*, 2007), of individual stable reflectors (*e.g.*, buildings, infrastructure, and rock outcrops).

While RAINS allowed the delineation of areas affected by displacement even in the absence of reflectors, MT-SBAS provided higher accuracy in the built-up areas.

Landslide mapping and cross-section

The integration of the datasets described above allowed the identification of three main "landslide sub-units" within the Brugneto landslide body. These sub-units were initially distinguished based on morphological evidence interpreted from the DTM and were further refined using surface displacement data from continuous GNSS and InSAR monitoring, considering both the temporal variability and the direction of movement. Material type and movement mechanism were also considered in the subdivision, with sub-units represented using a colour gradient to reflect their characteristics and surface displacement that distinguish them. In addition to the subunits, associated gravitational features, such as primary and secondary scarps, are reported. The cross-section line was selected to provide a clear representation of the geometric relationships among the sub-units, their spatiotemporal evolution, and the overlap of successive failure, depletion, and accumulation events. All available information, including geophysical surveys, boreholes, and inclinometer readings, was integrated into reference longitudinal cross-sections, illustrating the shape and extent of sub-units and elements separated by multiple deformation zones.

RESULTS

Electrical resistivity tomography (ERT) survey

The ERT1 profile was integrated into the A-A′ cross-section, with substantial overlap between the two datasets, and highlights marked lateral and vertical variability in resistivity, reflecting the heterogeneous internal structure of the landslide (Fig. 3). Low-resistivity zones are predominantly associated with fine-grained and water-saturated materials, whereas higher resistivity values correspond to coarser deposits and the underlying bedrock.

The ERT data allow the reconstruction of the subsurface geometry of the landslide body and its internal organization, suggesting the presence of multiple deformation zones. For completeness, the ERT2 profile is also shown, where its resistivity values indicate relatively moist sandy-silty deposits and the absence of bedrock down to approximately 30 m depth at that location. This information provides a useful constraint for interpreting the poorly investigated toe sector of the landslide.

Boreholes stratigraphy

Borehole data (4I, 6I, P2, P1, and 5P) provide essential ground-truth information for interpreting the electrical resistivity tomography survey (Fig. 3). The stratigraphic logs reveal heterogeneous sequences of fine- and coarse-grained materials overlying the bedrock, allowing a detailed definition of lithological boundaries. Borehole 4I does not reach the bedrock, which is absent in its stratigraphy, indicating that its depth is insufficient to fully constrain the landslide thickness and the deformation zone, which apparently could be under the borehole, like signed with the dashed arrow. In contrast, borehole 6I intercepts bedrock at 68 m depth, where fractured limestone is clearly identified (Fig. 3). Borehole P2 suggests the presence of a potential deformation zone at approximately 35 m depth.

This interpretation is supported by a corresponding low-resistivity anomaly in the ERT1 profile and by a chaotic horizon observed at a similar depth in borehole 6I, consistent with a deformation zone confirmed by inclinometric data. Boreholes P1 and 5P are also relatively shallow compared to the overall landslide thickness.

However, P1 records limestone at about 19 m depth, in agreement with a high-resistivity zone observed in the ERT1 section (Fig. 3). In contrast, 5P shows marked grain-size variability along its 21 m depth, likely reflecting its position in the landslide toe, where multiple depositional phases may have occurred over time. The integration of stratigraphic and resistivity data refines the subsurface reconstruction and constrains the depth of deformation zones, which are generally associated with chaotic or fractured lithologies, often consisting of coarser materials embedded within a finer-grained matrix.

Inclinometric monitoring

During the monitoring period from 17 April 2024 to 29 January 2026, inclinometer 4I, located upslope of the Brugneto village, recorded a cumulative displacement of 87.1 mm within a deformation zone between 20 and 25 m depth (Fig. 3). Since the

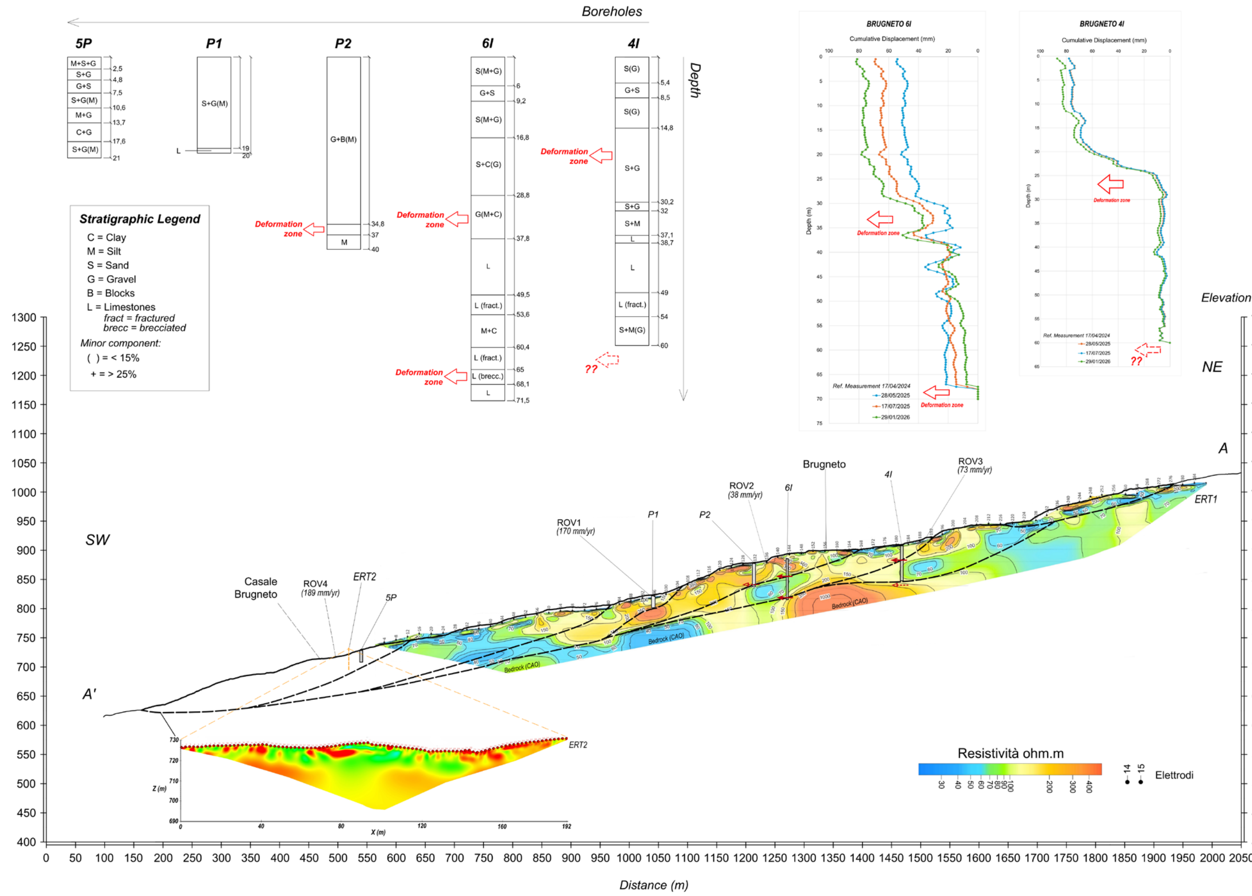

Fig. 3 - Integrated interpretation of ERT data (1-2-3), borehole stratigraphy, and inclinometric measurements along cross-section A-A'

borehole did not reach the bedrock, a deeper deformation level is expected, also considering the ERT1 results which shows resistivity changes below the elevation reached by the borehole. Over the same period of time, inclinometer 6I measured a cumulative displacement of 81.2 mm, identifying two main deformation zones: one between 30 and 35 m depth and a more localized zone at approximately 65 to 68 m, at the contact with bedrock (Fig. 3). The resulting displacement rates are approximately 40 mm/yr for inclinometer 4I and 37 mm/yr for inclinometer 6I. These data, combined with borehole stratigraphy, ERT1 and ERT2 results and geomorphological features, have been used for the delineation of the depth and geometry of multiple deformation zones along a cross-section, which shows a complex multiple sliding system.

Piezometric monitoring

Piezometric monitoring was conducted using diver loggers installed in piezometers 1P and 2P (Fig. 3). Piezometer 1P was monitored from 22 November 2022 to 6 February 2025 and remained mostly dry, with only occasional rises in groundwater reaching approximately 19.5 m below ground level. Piezometer 2P was monitored from 22 November 2022 to 29 August 2024, with a mean groundwater depth of about 39.3 m below ground level and limited fluctuations of around 0.20 m; from early spring 2024, it remained dry.

Manual measurements in piezometer 5P on 17 January 2025 indicated groundwater depths of approximately 12.2 m below ground level, and, in addition, 13.7 m in a nearby roadside well, located upslope near the Casale Brugneto hamlet.

Continuous GNSS monitoring

C-GNSS over the 2023-2025 period indicates increasing displacement rates from upslope to downslope along the landslide. From upslope to downslope: ROV3 0.15 m (73 mm/yr), ROV2 0.07 m (38 mm/yr), ROV1 0.35 m (170 mm/yr) and ROV4 0.40 m (189 mm/yr) (Fig. 4).

The displacement direction is toward the southwest for all C-GNSS rovers. Variations of displacement rates in time correlate quite directly with cumulative rainfall data from the Salsominore rain gauge, the nearest to the landslide (17 km south-southwest, elevation: 408 m a.s.l.; coordinates:

44.632711 N, 9.405315 E). Specifically, all the monitoring points show accelerated movements phases during the February to June period, when the cumulated rainfall during the previous 3 to 4 months exceed 300 to 400 mm.

In all circumstances, no significant response of the slope movements is recorded after short term-intense rainfalls.

MT-InSAR analysis

Results from MT-InSAR analysis over the October 2014 to March 2024 proved effective for the characterization of surface displacements. As a matter of fact, these results are substantially consistent with C-GNSS monitoring (although they tend to underestimate displacement rates) but allow for a much area-wide characterization of displacement rates and patterns. Specifically, MT-SBAS measurement points (MPs)

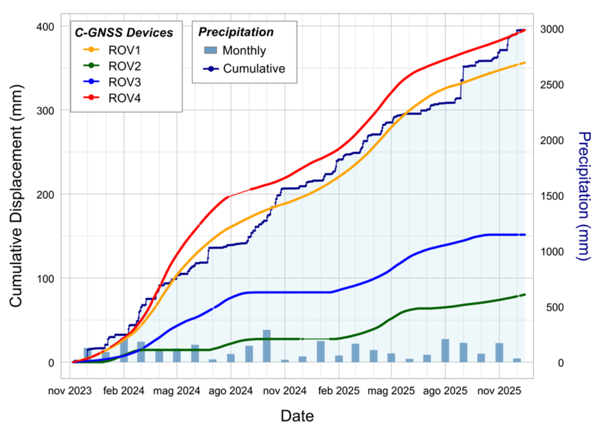

Fig. 4 - Cumulative planimetric displacement recorded by the C-GNSS stations (ROV3, ROV2, ROV1, ROV4) and corresponding monthly and cumulative rainfall at the Salsominore rain gauge during the monitoring period (2023-2025). Displacement rates increase from the upper to the lower sector of the Brugneto landslide

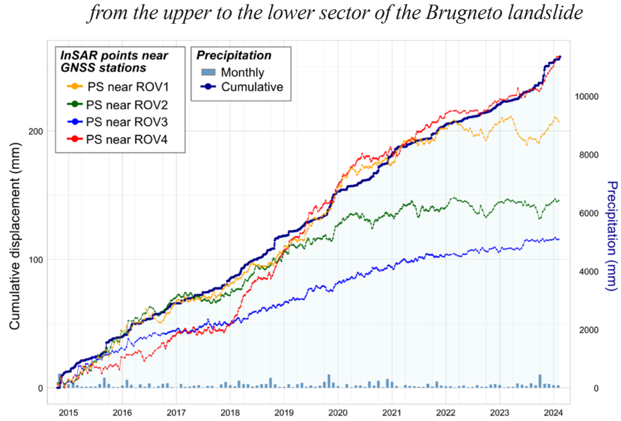

Fig. 5 - MT-SBAS displacement time series (2014-2024) for selected Permanent Scatterers located near the C-GNSS rovers, compared with monthly and cumulative precipitation recorded at the Salsominore rain gauge. Ascending-orbit displacements were sign-inverted to allow direct comparison with C-GNSS measurements

(mostly concentrated around the hamlet of Brugneto, due to the reflective nature of buildings) show significant and consistent movements affecting large part of the upper landslide area, and at location, also downslope in unbuilt areas (Fig. 5). At the same time, the results from RAINS show a more continuous spatial coverage at the slope scale, and evidence significantly higher displacement rates in the portion of the landslide from the hamlet of Brugneto down to the hamlet of Casale. In quantitative terms, a validation of MT-SBAS and RAINS results can be obtained by comparing displacement rates and trends associated to MPs located near the GNSS rovers. If time series are considered, the selected MPs from MT-SBAS in ascending orbit (the more favourable one in terms of Line of Sight vs. slope movements orientation) tend to underestimate displacement rates significantly (Fig. 6). The difference is more significant for MPs in the lower sector of the landslide (*i.e.* ROV1 and ROV4) and more limited in the upper portion of the slide (*i.e.* ROV2 and ROV3). In all cases, compared to C-GNSS measurements, landslide acceleration phases are less pronounced in the MT-SBAS time series and, also, their timing is erroneously biased toward the autumn to early winter period. This behaviour can be partly attributed to the long temporal span of the interferometric dataset, which tends to smooth short-term variations and reduce average velocity estimates, as also observed when comparing short-term and long-term interferometric stacks. Moreover, during periods of rapid movement, displacement rates may exceed the sensitivity limits of the interferometric technique, further contributing to the underestimation. Although RAINS provides displacement rates closer to C-GNSS than MT-SBAS, it still underestimates absolute values. Overall, these discrepancies reflect intrinsic limitations of InSAR techniques, including phase cycle slips and the Line-of-Sight (LoS) measurement geometry, which captures only a component of the actual displacement vector. Despite these limitations, MPs located near ROV1 and ROV4 consistently show the highest variability over time, in agreement with C-GNSS observations, confirming the reliability of MT-InSAR data in capturing the main spatial and temporal patterns of landslide activity.

	Mean Velocity [mm/yr]				
Reference Points	GNSS	SBAS *Asc*	SBAS *Desc*	RAINS *Asc*	RAINS *Desc*
ROV1	170.53	-23.64	19.07	-47.1	48.88
ROV2	38.37	-14.1	12	-13.29	29.47
ROV3	73.33	-10.76	12.57	-19.87	21.7
ROV4	188.6	-9.65	2.93	-28.23	-8.25

Tab. 1 - Comparison of average annual displacement rates derived from continuous GNSS monitoring and InSAR analyses (MT-SBAS and RAINS) at locations proximal to the GNSS rover stations along the Brugneto landslide

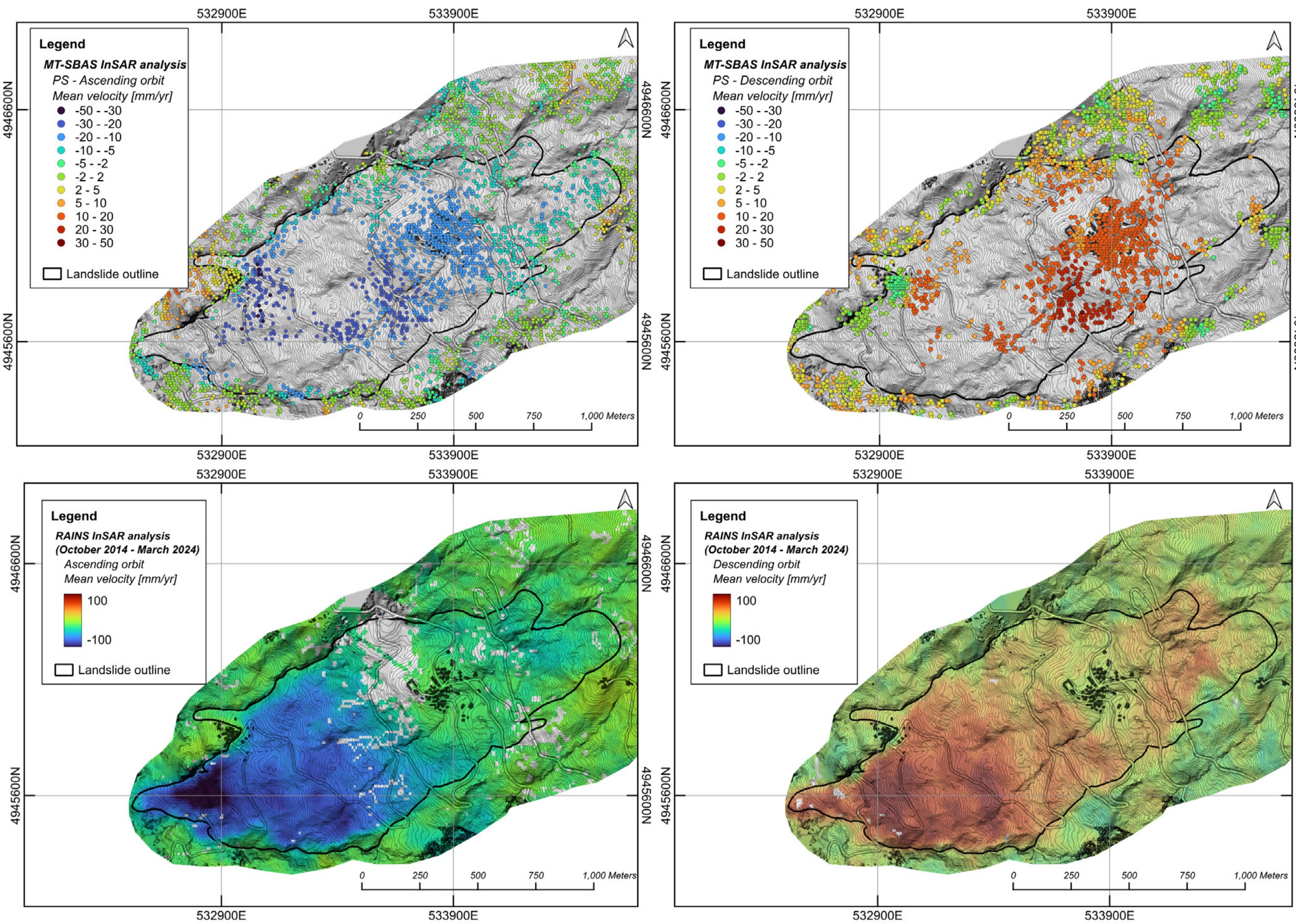

Fig. 6 - Slope movement rates derived from MT-SBAS and RAINS interferometry using Sentinel 1 data in the 2014-2024 period

LANDSLIDE MAP AND CROSS-SECTION

The integration of all available datasets allowed the production of a geological map with a reference longitudinal cross-section (Fig. 7). The map subdivides the landslide into 3 main sub-units, characterised by distinct geological, kinematic, and morphological features (Table 2). The geological and monitoring evidence indicate a progressive transition from roto-translational rock slides in the upper sector (sub-units A and B) to translational earth slide in the lowermost sub-unit (C). A colour gradient was adopted in the map to indicate higher or lower displacement rates resulting from C-GNSS and MT-SBAS and RAINS monitoring. The geological cross-section provides a representation of the geometric and kinematic relationships among sub-units. Upslope, the landslide detachment area appears to be controlled by the bedding orientation of the CAO Flysch, which locally displays a syncline and anticline structure, with bedding planes resulting slightly steeper than the slope in the upper part of the landslide. Moving downslope, the evidence of higher displacement rates in ROV3 than in ROV2, can be interpreted by assuming that sub-unit A overthrusts sub-

Sub-Unit	A	B	C
Slide Kinematics	Roto-Transl.	Roto-Transl.	Transl.
Material (Formation)	Rock (CAO)	Rock (CAO)	Earth (block in matrix)
Area (km^2)	0.22	0.32	0.65
Length max (km)	0.63	0.66	1,1
Width max (km)	0.45	0.8	0.82
L/W ratio	1.4	0.8	1.4
Slope avg. (°)	20	16	17
Depth max (m)	40	70	70
Volume (Mm^3)	~8.0	~20.0	~40.0

Tab. 2 - Main characteristics of the Brugneto landslide sub-units

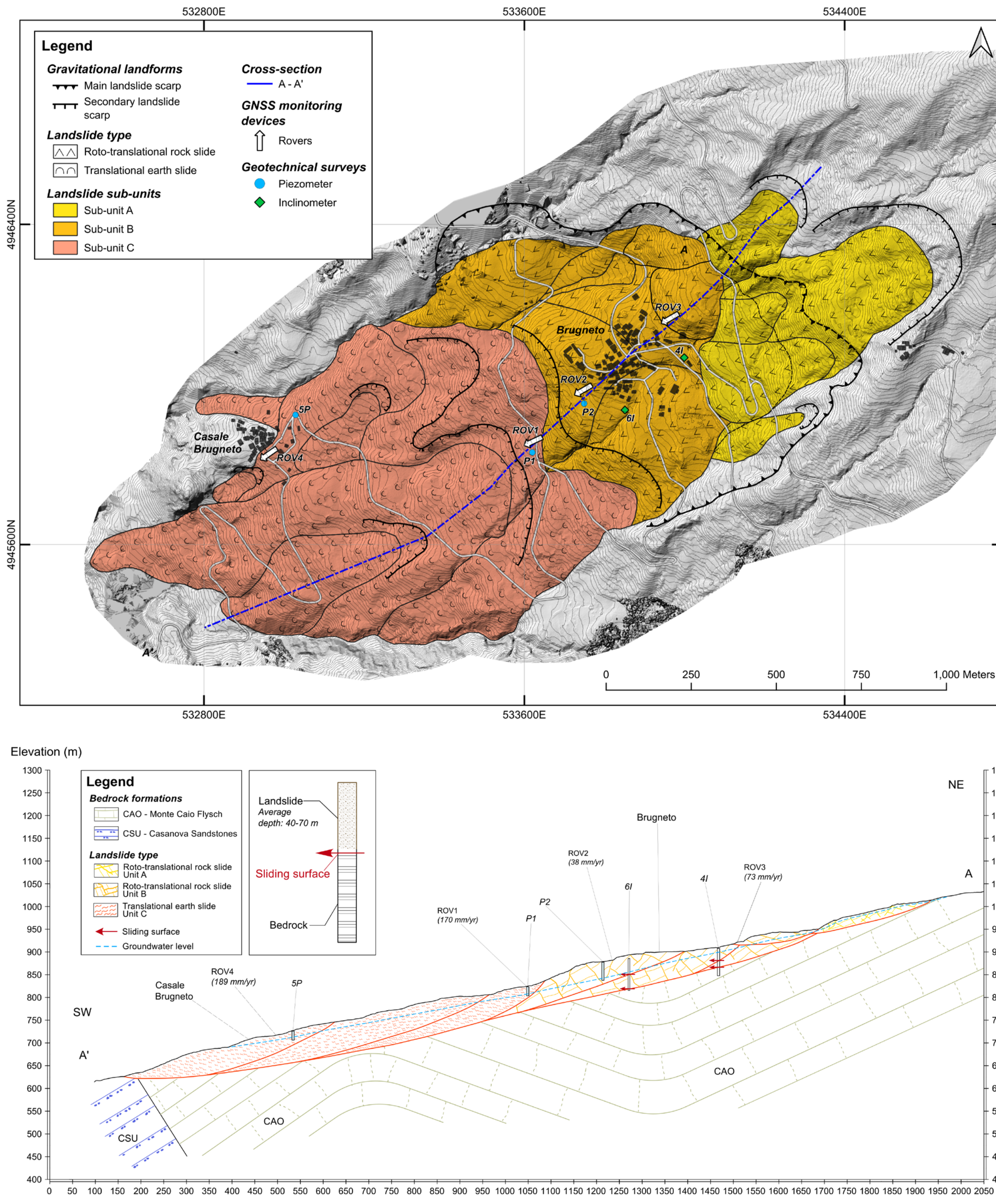

Fig. 7 - Geological model of the Brugneto landslide. Map (top) showing the delineation of sub-units within the landslide body, and reference geological cross-section A-A' (bottom), illustrating the relationships among the identified sub-units, the multiple sliding surfaces recorded by inclinometers, and groundwater levels measured using piezometers. Monitoring instruments not located directly on the section track were projected onto it, to provide additional data for a more detailed and representative geological cross-section

unit B. In turn, sub-unit B is considered to be dissected and further mobilized by sub-unit C, which is justified by the presence of quite evident secondary scarps and by the higher displacement rates recorded in ROV1 and ROV4 than in ROV2. The depth of the multiple deformation zones affecting sub-unit B are quite precisely constrained by inclinometer data, which show movements down to a maximum depth of approximately 70 m. Conversely, the depth of the basal sliding surface in sub-unit C has been inferred on the basis of the morphometric characteristics of the landslide and on the basis of the ERT1 profile (in the upper part) and, also, of ERT2 profile (in the lower part). However, due to the limited spatial coverage of surveys and the lack of direct investigations down to the bedrock, the delineation of sliding surfaces inside sub-unit C, presented in the cross-section of Fig. 7, is substantially inferred on the basis of geomorphic evidences of separated landslide units forming a multiple sliding system. A more precise delineation will require further investigation by deep boreholes drilling and additional inclinometers. It should be noted that in the reference geological cross-section, some monitoring instruments and features were not located directly along the section track but were projected onto it, as also observed in the Brugneto landslide map (Fig. 7). This approach allowed the integration of additional data to refine and better constrain the representative geological cross-section. Finally, the C-GNSS monitoring data indicate a correlation between displacement rates and multi-monthly cumulative rainfall patterns, pointing to a deep-groundwater recharge control of the landslide kinematics. Although groundwater monitoring data are limited, the available piezometric measurements indicate a groundwater table relatively close to the ground surface. Despite the lack of robust and continuous data, these measurements proved useful for the reconstruction of a conceptual piezometric surface within the landslide body, obtained by interpolating the groundwater levels recorded in the piezometers and subsequently incorporated into the geological cross-section A-A' (Fig. 7). Further investigations, including the installation of additional and deeper piezometers, are required to better constrain the depth, geometry, and spatial variability of the groundwater system.

CONCLUSIONS

The integrated investigation and monitoring of the Brugneto landslide supported the development of a reference geological and kinematical model for this complex deep-seated slope failure. The landslide consists of three main sub-units, each characterized by distinct movement mechanisms and deformation zones reaching depths of up to 70 m. Overall, deformation remains relatively steady, with episodic accelerations during the winter-spring period linked to prolonged cumulative rainfall. MT-InSAR and C-GNSS datasets exhibit broadly consistent spatial and temporal patterns, although they diverge in displacement rates and short-term variability, particularly in the most recent monitoring phase. These differences arise from intrinsic methodological factors: InSAR measures only the Line-of-Sight component of motion and is affected by temporal smoothing, which reduces sensitivity to rapid acceleration. Consequently, MT-InSAR tends to underestimate rates and reduce short-term fluctuations, whereas C-GNSS provides more precise and temporally detailed measurements. Despite these contrasts, the combined use of both techniques proves highly effective, merging the spatial continuity of MT-InSAR with the accuracy of *in situ* GNSS to achieve a comprehensive reconstruction of landslide kinematics.

A notable limitation of the study is the relatively sparse data coverage in the landslide toe, which constrains the characterization and geological modelling of the terminal sector. Future work will focus on expanding the monitoring network in this area and beyond, to refine subsurface reconstruction, strengthen the proposed geological model, and better characterize a phenomenon of this spatial extent. In summary, the work demonstrates the value of integrating multiple monitoring techniques for analysing deep-seated landslides in structurally and lithologically heterogeneous settings, such as the Northern Apennines and other comparable geological environments. Nevertheless, even with extensive datasets, fully characterizing a phenomenon of this scale and structural heterogeneity remains challenging.

REFERENCES

Agliardi F., Crosta G. & Zanchi A. (2001) - *Structural constraints on deep-seated slope deformation kinematics*. Engineering Geology, **59**: 83-102. https://doi.org/https://doi.org/10.1016/S0013-7952(00)00066-1

Allasia P., Godone D., Giordan D., Guenzi D. & Lollino G. (2020) - *Advances on measuring deep-seated ground deformations using robotized inclinometer system*. Sensors, **20**(13): 3769. https://doi.org/10.3390/s20133769

Arosio D., Brambilla D., Longoni L., Papini M., Savazzi G. & Zanzi L. (2011) - *Integration of geological and geophysical data to improve the understanding of a deep-seated landslide*. Symposium on the Application of Geophysics to Engineering and Environmental Problems 2011: 166-166. https://doi.org/10.4133/1.3614285

Bertolini G., Corsini A. & Tellini C. (2017) - *Fingerprints of large-scale landslides in the landscape of the Emilia Apennines*. In World Geomorphological Landscapes: 215-224. Springer. https://doi.org/10.1007/978-3-319-26194-2_18

Bonzanigo L., Eberhardt E. & Loew S. (2007) - *Long-term investigation of a deep-seated creeping landslide in crystalline rock*. Part I. *Geological and hydromechanical factors controlling the Campo Vallemaggia landslide*. Canadian Geotechnical Journal, **44**(10): 1157-1180. https://doi.org/10.1139/T07-043

Borgatti L., Corsini A., Barbieri M., Sartini G., Truffelli G., Caputo G. & Puglisi C. (2006) - *Large reactivated landslides in weak rock masses: A case study from the Northern Apennines (Italy).* Landslides, **3**(2): 115-124. https://doi.org/10.1007/s10346-005-0033-9

Bürgmann R., Rosen P. A. & Fielding E. J. (2000) - *Synthetic aperture radar interferometry to measure earth's surface topography and its deformation*. Annual Review of Earth and Planetary Sciences, **28**(1): 169-209. https://doi.org/10.1146/annurev.earth.28.1.169

Carrara A., Crosta G. & Frattini P. (2003) - *Geomorphological and historical data in assessing landslide hazard.* Earth Surface Processes and Landforms, **28**(10): 1125-1142. https://doi.org/10.1002/esp.545

Chelli A., Bordoni M., Cappadonia C., Pepe G., Rotigliano E. & Smith M. (2021) - *Geomorphological tools for mapping natural hazards.* Journal of Maps, **17**(3): 1-4. https://doi.org/10.1080/17445647.2021.1920794

Ciccarese G., Tondo M., Mulas M., Bertolini G. & Corsini A. (2024) - *Rapid assessment of landslide dynamics by UAV-RTK repeated surveys using ground targets: the Ca' Lita Landslide (Northern Apennines, Italy).* Remote Sensing, **16**(6). https://doi.org/10.3390/rs16061032

Ciuffi P., Bayer B., Berti M., Franceschini S. & Simoni A. (2024) - *InSAR stacking to detect active landslides and investigate their relation to rainfalls in the Northern Apennines of Italy*. Geomorphology, **457**: 109242. https://doi.org/10.1016/j.geomorph.2024.109242

Corominas J., Van Westen C., Frattini P., Cascini L., Malet J. P., Fotopoulou S., Catani F., Van Den Eeckhaut M., Mavrouli O., Agliardi F., Pitilakis K., Winter M. G., Pastor M., Ferlisi S., Tofani V., Hervás J. & Smith J. T. (2014) - *Recommendations for the quantitative analysis of landslide risk. Bulletin of Engineering Geology and the Environment*, **73**(2): 209-263. https://doi.org/10.1007/s10064-013-0538-8

Corsini A., Bonacini F., Mulas M., Petitta M., Ronchetti F. & Truffelli G. (2015) - *Long-Term Continuous Monitoring of a Deep-Seated Compound Rock Slide in the Northern Apennines (Italy)*. In: G. Lollino D. Giordan, G. B. Crosta, J. Corominas, R. Azzam, J. Wasowski & N. Sciarra (Eds.), *Engineering Geology for Society and Territory*, **2**: 1337-1340. Springer International Publishing. https://doi.org/10.1007/978-3-319-09057-3_235

Corsini A., Bonacini F., Mulas M., Ronchetti F., Monni A., Pignone S., Primerano S., Bertolini G., Caputo G., Truffelli G., Benini A. & Berti M. (2015) - *A portable continuous GPS array used as rapid deployment monitoring system during landslide emergencies in Emilia Romagna.* Rendiconti Online Della Società Geologica Italiana, **35**: 89-91. https://doi.org/10.3301/ROL.2015.71

Corsini A., Borgatti L., Pellegrini M., Ronchetti F., Borghi A., Campagnoli I., Caputo G., Gatti A., Leuratti E., Lucente C., Truffell G. & Sartini G. (2005) - *Monitoraggio di grandi frane riattivate e sospese nella valle del Fiume Secchia (Appennino settentrionale)*. Giornale Di Geologia Applicata, **2**: 35-44. https://doi.org/10.1474/GGA.2005-02.0-05.0031

Crosta G. B., Frattini P. & Agliardi F. (2013) - *Deep seated gravitational slope deformations in the European Alps*. Tectonophysics, **605**: 13-33. https://doi.org/10.1016/j.tecto.2013.04.028

Cruden D. M. & Varnes D. (1996) - *Landslide types and processe*s. In: Turner A.K. & Schuster R.L. (Eds.), *Landslides: Investigation and Mitigation*: 36-75. Transportation Research Board, National Research Council, Special Report, Washington DC.

Del Soldato M., Riquelme A., Bianchini S., Tomàs R., Di Martire D., De Vita P., Moretti S. & Calcaterra D. (2018) - *Multisource data integration to investigate one century of evolution for the Agnone landslide (Molise, southern Italy)*. Landslides, **15**(11): 2113-2128. https://doi.org/10.1007/s10346-018-1015-z

Dewitte O. & Demoulin A. (2005) - *Morphometry and kinematics of landslides inferred from precise DTMs in West Belgium*. Natural Hazards and Earth System Sciences, **5**(2): 259-265. https://doi.org/10.5194/nhess-5-259-2005

Donnini M., Bucci F., Santangelo M., Cardinali M. & Reichenbach P. (2025) - *The effect of different landslide mapping approaches on the geomorphological assessment of landslide hazard*. https://doi.org/10.5194/egusphere-2025-2096

Elter P., Ghiselli F., Marroni M. & Ottria G. (1997) - *Note illustrative della Carta Geologica d'Italia in scala 150.000 - Foglio 197, "Bobbio*". In Istituto Poligrafico e Zecca dello Stato, Roma.

Fiolleau S., Uhlemann S., Wielandt S. & Dafflon B. (2023) - Understanding slow-moving landslide triggering processes using low-cost passive seismic and inclinometer monitoring. Journal of Applied Geophysics, **215**. https://doi.org/10.1016/j.jappgeo.2023.105090

Glabsch J., Heunecke O. & Schuhbäck S. (2009) - Monitoring the Hornbergl landslide using a recently developed low cost GNSS sensor network. Journal of Applied Geodesy, **3**(3): 259-265. https://doi.org/10.1515/JAG.2009.019

Guzzetti F., Carrara A., Cardinali M. & Reichenbach P. (1999) - Landslide hazard evaluation: a review of current techniques and their application in a multi-scale study, Central Italy. Geomorphology, **31**(1-4): 181-216. https://doi.org/10.1016/S0169-555X(99)00078-1

Guzzetti F., Mondini A. C., Cardinali M., Fiorucci F., Santangelo M. & Chang K. T. (2012) - *Landslide inventory maps: New tools for an old problem*. Earth-Science Reviews, **112**(1-2): 42-66. https://doi.org/10.1016/j.earscirev.2012.02.001

Jaboyedoff M., Oppikofer T., Abellán A., Derron M. H., Loye A., Metzger R. & Pedrazzini A. (2012) - *Use of LIDAR in landslide investigations: A review.* Natural Hazards, **61**(1): 5-28. https://doi.org/10.1007/s11069-010-9634-2

Johnson S. E., Haneberg W. C., Bryson L. S. & Crawford M. M. (2023) - *Measuring ground surface elevation changes in a slow-moving colluvial landslide using combinations of regional airborne lidar, UAV lidar and UAV photogrammetric surveys*. Quarterly Journal of Engineering Geology and Hydrogeology, **56**(2). https://doi.org/10.1144/qjegh2022-078

Jongmans D. & Garambois S. (2007) - *Geophysical investigation of landslides : a review*. Bulletin de La Société Géologique de France, **178**(2): 101-112.

https://doi.org/10.2113/gssgfbull.178.2.101

Lacroix P., Handwerger A. L. & Bièvre G. (2020) - *Life and death of slow-moving landslides*. Nature Reviews Earth & Environment, **1**(8): 404-419. https://doi.org/10.1038/s43017-020-0072-8

Lanari R., Casu F., Manzo M., Zeni G., Berardino P., Manunta M. & Pepe A. (2007) - *An overview of the small baseline subset algorithm: A DInSAR technique for surface deformation analysis.* In: Deformation and Gravity Change: Indicators of Isostasy, Tectonics, Volcanism, and Climate Change: 637-661. Birkhäuser Basel. https://doi.org/10.1007/978-3-7643-8417-3_2

Lee E. M. (2001) - *Geomorphological mapping*. Geological Society Special Publication, **18**: 53-56. https://doi.org/10.1144/gsl.eng.2001.018.01.08

Lelli F., Mulas M., Critelli V., Fabbiani C., Tondo M., Aleotti M. & Corsini A. (2025) - *Leveraging High-Frequency UAV–LiDAR Surveys to Monitor Earthflow Dynamics—The Baldiola Landslide Case Study.* Remote Sensing, **17**(15). https://doi.org/10.3390/rs17152657

Luhn J., Stumvoll-Schmaltz M. J., Orozco A. F. & Glade T. (2023) - *Internal structure of an active landslide based on ERT and DP data: New insights from the Hofermühle landslide observatory in Lower Austria.* Geomorphology, **441**. https://doi.org/10.1016/j.geomorph.2023.108910

Mantovani M., Bossi G., Dykes A. P., Pasuto A., Soldati M. & Devoto S. (2022) - *Coupling long-term GNSS monitoring and numerical modelling of lateral spreading for hazard assessment purposes*. Engineering Geology, **296**. https://doi.org/10.1016/j.enggeo.2021.106466

Massonnet D. & Feigl K. L. (1998) - *Radar interferometry and its application to changes in the Earth's surface.* Reviews of Geophysics, **36**(4): 441-500. https://doi.org/10.1029/97RG03139

Mulas M., Ciccarese G., Ronchetti F., Truffelli G. & Corsini A. (2018) - *Slope dynamics and streambed uplift during the Pergalla landslide reactivation in March 2016 and discussion of concurrent causes (Northern Apennines, Italy).* Landslides, **15**(9): 1881-1887. https://doi.org/10.1007/s10346-018-1039-4

Mulas M., Ciccarese G., Truffelli G. & Corsini A. (2020a) - *Displacements of an active moderately rapid landslide—A dataset retrieved by continuous gnss arrays.* Data, **5**(3): 1-6. https://doi.org/10.3390/data5030071

Mulas M., Ciccarese G., Truffelli G. & Corsini A. (2020b) - *Integration of digital image correlation of Sentinel-2 Data and Continuous GNSS for long-term slope movements monitoring in moderately rapid landslides.* Remote Sensing, **12**(16): 2605. https://doi.org/10.3390/rs12162605

Pánek T. & Klimeš J. (2016) - *Temporal behavior of deep-seated gravitational slope deformations: A review.* Earth-Science Reviews, **156**: 14-38. https://doi.org/10.1016/j.earscirev.2016.02.007

Parry S. (2011) - *The Application of Geomorphological Mapping in the Assessment of Landslide Hazard in Hong Kong.* Developments in Earth Surface Processes, **15**(2011): 413-441. https://doi.org/10.1016/B978-0-444-53446-0.00015-X

Pastor J. L., Tomás R., Lettieri L., Riquelme A., Cano M., Infante D., Ramondini M. & Di Martire D. (2019) - *Multi-Source Data Integration to Investigate a Deep-Seated Landslide Affecting a Bridge.* Remote Sensing, **11**(16): 1878. https://doi.org/10.3390/rs11161878

Pasuto A. & Soldati M. (1999) - *The use of landslide units in geomorphological mapping: an example in the Italian Dolomites.* Geomorphology, **30**: 53-64.

Petley D. N. & Allison R. J. (1997) - *The mechanics of deep-seated landslides.* Earth Surface Processes and Landforms, **22**: 747-758. https://doi.org/https://doi.org/10.1002/(SICI)1096-9837(199708)22:8%3C747::AID-ESP767%3E3.0.CO;2-%23

Roccati A., Paliaga G., Luino F., Faccini F. & Turconi L. (2021) - *Gis-based landslide susceptibility mapping for land use planning and risk assessment*. Land, **10**(2): 1-28. https://doi.org/10.3390/land10020162

Rosen P. A., Hensley S., Joughin I. R., Li F. K., Madsen S. N., Rodriguez E. & Goldstein R. M. (2000) - *Synthetic aperture radar interferometry*. Proceedings of the IEEE, **88**(3): 333-382. https://doi.org/10.1109/5.838084

Sacchini A., Faccini F., Ferraris F., Firpo M. & Angelini S. (2016) - *Large-scale landslide and deep-seated gravitational slope deformation of the Upper Scrivia Valley (Northern Apennine, Italy).* Journal of Maps, **12**(2): 344-358. https://doi.org/10.1080/17445647.2015.1021393

Simeoni L. & Ferro E. (2015) - *Displacement rates of extremely slow landslides*. Proceedings of the XVI ECSMGE Geotechnical Engineering for Infrastructure and Development. https://doi.org/10.1680/ecsmge.60678

Simeoni L., Ronchetti F., Costa C., Joris P. & Corsini A. (2020) - *Redundancy and coherence of multi-method displacement monitoring data as key issues for the analysis of extremely slow landslides (Isarco valley, Eastern Alps, Italy)*. Engineering Geology, **267**: 105504. https://doi.org/10.1016/j.enggeo.2020.105504

Sterzai P., Vellico M., Berti M., Coren F., Corsini A., Rosi A., Mora P., Zambonelli F. & Ronchetti F. (2010) - *LiDAR and hyperspectral data integration for landslide monitoring: The test case of valoria landslide.* Italian Journal of Remote Sensing / Rivista Italiana Di Telerilevamento, **42**(3): 89-99. https://doi.org/10.5721/itjrs20104237

Tofani V., Hong Y. & Singhroy V. (2014) - *Introduction: Remote Sensing Techniques for Landslide Mapping and Monitoring*. In: Landslide Science for a Safer Geoenvironment: 301-303. Springer International Publishing. https://doi.org/10.1007/978-3-319-05050-8_47

Van Westen C. J. & Lulie Getahun F. (2003) - *Analyzing the evolution of the Tessina landslide using aerial photographs and digital elevation models.* Geomorphology, **54**(1-2): 77-89. https://doi.org/10.1016/S0169-555X(03)00057-6

Van Westen C. J., Rengers N. & Soeters R. (2003) - *Use of Geomorphological Information in Indirect Landslide Susceptibility Assessment.* Natural Hazards, **30**(3): 399-419. https://doi.org/10.1023/B:NHAZ.0000007097.42735.9e

Wieczorek G.F. (1996) - *Landslide triggering mechanisms*. In: Turner A.K. & Schuster R.L. (Eds.), *Landslides: Investigation and Mitigation*, **247**: 76-90.

Transportation Research Board, National Research Council, Special Report, Washington DC.

Zangerl C., Eberhardt E. & Perzlmaier S. (2010) - *Kinematic behaviour and velocity characteristics of a complex deep-seated crystalline rockslide system in relation to its interaction with a dam reservoir*. Engineering Geology, **112**(1-4): 53-67. https://doi.org/10.1016/j.enggeo.2010.01.001

Received January 2026 - Accepted April 2026